Article:
Harris, Benjamin and Wagenaars, Erik (2023) The influence of pulse repetition frequency on reactive oxygen species production in pulsed He+H2O plasmas at atmospheric pressure. Journal of Applied Physics. 103302. ISSN: 1089-7550

https://doi.org/10.1063/5.0161825

Journal of Applied Physics

RESEARCH ARTICLE | SEPTEMBER 12 2023

The influence of pulse repetition frequency on reactive oxygen species production in pulsed He+H_2O plasmas at atmospheric pressure

B. Harris ; E. Wagenaars

J. Appl. Phys. 134, 103302 (2023)
https://doi.org/10.1063/5.0161825

AIP Publishing

Journal of Applied Physics ARTICLE pubs.aip.org/aip/jap

The influence of pulse repetition frequency on reactive oxygen species production in pulsed He+H_2O plasmas at atmospheric pressure

Cite as: J. Appl. Phys. **134**, 103302 (2023); doi: 10.1063/5.0161825
Submitted: 12 June 2023 · Accepted: 24 August 2023 ·
Published Online: 12 September 2023

B. Harris[a] and E. Wagenaars

AFFILIATIONS

York Plasma Institute, School of Physics, Engineering and Technology, University of York, Heslington, York YO10 5DD, United Kingdom

[a]**Author to whom correspondence should be addressed:** benjamin.harris@york.ac.uk

ABSTRACT

Atmospheric pressure plasmas generated from a helium gas with admixtures of water vapor have numerous applications in biomedicine. It is important that the chemistry of such plasmas can be tightly controlled so that they may be tailored for their intended use. In this study, computational modeling is used to vary the pulse repetition frequency of a nanosecond-pulsed, pin-to-pin He + 0.25% H_2O discharge in the range of 1–100 kHz to determine the influence of the pulse repetition frequency on the resulting densities of reactive oxygen species and the rates of dominant reaction pathways involving them. The plasma is simulated using the 0D plasma-chemical kinetics model GlobalKin. The pulse shape is kept constant. The afterglow duration is, therefore, dependent on the repetition frequency. Analysis of the bulk plasma chemistry after the plasma has reached equilibrium shows that the peak electron density is only weakly dependent on the pulse repetition frequency. Increasing the pulse repetition frequency is shown to increase the density of H, O, and OH radicals, while the relationship between the repetition frequency and the densities of species with longer lifetimes, namely, H_2O_2 and O_3, is found to be more complex. These are formed throughout the afterglow, and their density depends on the availability of reactant species, the afterglow duration, and the background gas temperature. This work concludes that the pulse repetition frequency is not a simple control parameter, especially for species that are predominantly produced in the afterglow. Detailed modeling is required for accurate control of species densities using the pulse repetition frequency.

I. INTRODUCTION

Low temperature plasmas generated at atmospheric pressure have seen great interest in recent years due to their ability to be operated in ambient air and close to room temperature.[1–8] These properties make them well suited to biomedical applications, including cancer therapy, microbial sterilization, and the treatment of chronic wounds.[9–11] If small admixtures of oxygen or water vapor are introduced to the feed gas, the electron-driven plasma chemistry can produce high densities of reactive oxygen species (ROS). The resulting mixture of species can exhibit a complex array of effects on the human body; for example, the OH radical is highly reactive and readily oxidizes proteins and DNA molecules, causing cell damage and instability in healthy and cancerous tissues alike.[12] H_2O_2 primarily acts as a cell signaling molecule, mediating immune responses.[13] Depending on its concentration, it can also inhibit the growth of bacterial infections, while at too high a dose, it causes damage to human cells due to oxidative stress.[14] Like H_2O_2, O_3 is known to stimulate the immune system and inactivate micro-organisms; however, it is toxic in high concentrations.[15] Given this array of functionality, it is evident that the plasma chemistry must be tightly controlled when optimizing a plasma for a specific application.

O_3 is produced in abundance in helium plasmas with admixtures of O_2, and thanks to extensive research, the mechanisms governing this are now well understood.[16–19] Similarly, helium plasmas with admixtures of H_2O have garnered attention due to their ability to produce tunable amounts of H_2O_2 and OH.[6,8,20] It has also been established that these two admixtures can be used in

tandem, with $He+O_2+H_2O$ plasmas offering a high degree of selectivity between hydrogen-containing species and those containing only oxygen.[2,21,22]

For discharges operated with pulsed power schemes, the number of pulses per second can be modified, while the pulse itself is left unchanged. This parameter, the pulse repetition frequency, presents a seemingly straightforward way of tuning the plasma chemistry. This is due in part to the parameter being altered by purely electrical means. The lack of mechanical action reduces the risk of component wear over time, while also allowing the plasma chemistry to be modified at a rate restricted only by the effluent transit time. Previous works have investigated the use of pulse repetition frequency as a control parameter for pulsed-power atmospheric pressure plasmas. The influence of pulse repetition frequency on discharge behavior[23,24] and electron parameters[25,26] in dielectric barrier discharges has been reported, in addition to its effects on efficiency and selectivity in the conversion of methane and CO_2.[27] It has also been demonstrated that the repetition frequency of $He+O_2$ plasmas can be altered to improve their effectiveness in biomedical roles, such as for triggering apoptosis in cancerous cells[28] or for treating tissue beneath a thin layer of liquid.[29]

When considering pulsed plasma sources, operation with nanosecond-scale pulses can efficiently generate energetic electrons, driving an active plasma chemistry while also suppressing excessive gas heating due to the long afterglow period relative to the pulse.[30] Fundamental studies have been conducted that investigate the influence of pulse repetition frequency on atmospheric pressure, nanosecond-pulsed plasmas for a number of gas compositions, including helium,[31] air,[32,33] $Ar+CH_4$,[30,34] Ne+Ar,[35] H_2+air,[36] and CH_4+air.[37] However, the influence of pulse repetition frequency on ROS production, and the overall plasma chemistry, in the bulk of a $He+H_2O$ plasma has not yet been studied in detail. This paper presents a model study in which the pulse repetition frequency is varied so as to characterize its effect on ROS production across the power cycle.

II. MODEL DESCRIPTION

A. GlobalKin

A $He+H_2O$ plasma is simulated using the 0D plasma-chemical kinetics model GlobalKin, described in detail in Ref. 38. To summarize, GlobalKin computes plasma processes iteratively with user-defined time steps. A chemistry and transport module constructs an ordinary differential equation (ODE) for the density of each species included in the model, describing their rate of change with respect to time. These density ODEs fit the form

$$\frac{dn_i}{dt} = \sum_j \left\{ \left(a_{ij}^R - a_{ij}^L\right) k_j \prod_l n_l^{a_{ij}^L} \right\} + \frac{S}{V}\left(-\frac{D_i n_i \gamma_i}{\gamma_i \Lambda + \frac{4D_i}{v_{th,i}}} + \sum_j \frac{D_j n_j \gamma_j f_{ji}}{\gamma_j \Lambda + \frac{4D_j}{v_{th,j}}} \right), \quad (1)$$

where n is the number density of species i. The first term describes the gas phase chemistry, where a_{ij}^R is the stoichiometric coefficient of species i in reaction j on the right-hand side of the reaction and a_{ij}^L is the stoichiometric coefficient on the left-hand side. The bracketed term is, therefore, the difference between these coefficients, giving the change in species i per reaction. k_j is the rate coefficient of reaction j, and $\prod_l n_l^{a_{ij}^L}$ accommodates for the reaction partners. The second term quantifies the gain and loss of particles due to collisions with the vessel wall, where $\frac{S}{V}$ is the surface area to volume ratio of the plasma, D is the diffusion coefficient, γ is the sticking coefficient of a heavy particle colliding with the reactor wall, Λ is the diffusion length, v_{th} is the thermal velocity of the particle, and f is the return fraction of a species from the walls.

The chemistry and transport module also constructs ODEs to describe the rate of change in the electron and gas temperatures. The electron temperature ODE is as follows:

$$\frac{d}{dt}\left(\frac{3}{2} n_e k_B T_e\right) = P_e - \sum_i \frac{3}{2} n_e \nu_{mi} \left(\frac{2m_e}{M_i}\right) k_B (T_e - T_i) + \sum_l n_e k_l n_l \Delta\varepsilon_l, \quad (2)$$

where n_e is the electron density, k_B is the Boltzmann constant, T_e and T_i are the electron and neutral gas temperatures, P_e is the power supplied to the electrons at time t, ν_{mi} is the momentum transfer collision frequency, m_e and M_i are the electron and heavy particle masses, k_l is the rate coefficient of reaction l, n_l is the density of the collision partner in reaction l, and $\Delta\varepsilon_l$ is the change in electron energy due to the collision. These are arranged such that the left-hand side of the equation describes the rate of change in the total kinetic energy of the electrons. The first term on the right-hand side gives the rate of electron energy gain through power deposition. The second and third terms describe the energy exchange through elastic and inelastic collisions, respectively, with heavy particles. The gas temperature is estimated using a simplified form of the equation described in Ref. 38. In this case, the gas temperature T_g is calculated by considering the balance of the power deposition and conductive heat losses,

$$\frac{d}{dt}\left(\frac{3}{2} N_g c_p T_g\right) = P_{ion} - \frac{\kappa}{\Lambda^2}(T_g - T_w), \quad (3)$$

where N_g, c_p, and κ are the gas mixture's total density, specific heat, and thermal conductivity, respectively. P_{ion} is the power supplied to the ions at time t, and T_w is the temperature of the bounding surfaces. Equations (1)–(3) are passed to an ODE solver module, which extracts the relevant parameters and passes them back to the chemistry and transport module for the next iteration. A Boltzmann solver module is also periodically called to solve a two-term approximation of the Boltzmann equation, allowing the rates of electron impact reactions and corresponding diffusion coefficients to be updated. This module is called less frequently than the ODE solver to save on processing power, as very small changes in the electron energy distribution function should have minimal impact on the overall plasma chemistry.

B. Model parameters

In this study, GlobalKin is supplied with a chemistry set containing 46 species and 577 reactions covering He, H_2O, and O_2 gas

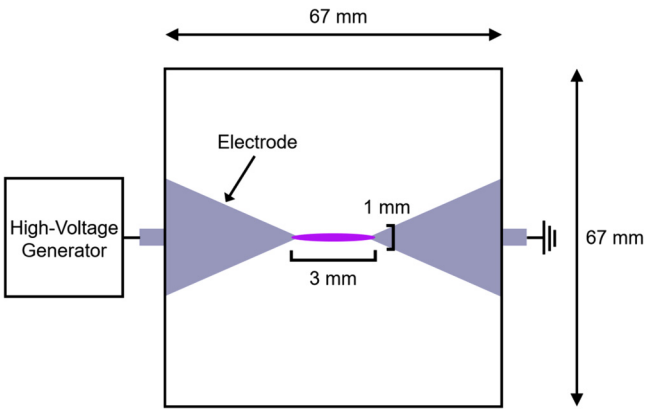

FIG. 1. Cross section of the discharge setup and the containment vessel.

mixtures, listed in Ref. 2. This chemistry set has been validated in previous studies against experimental measurements of O and OH densities, alongside time-resolved electron density measurements.[2,39] Despite being a spatially averaged model, GlobalKin requires geometric inputs in the forms of the surface-area-to-volume ratio and radius of the plasma. As such, the dimensions used in this model were matched to an existing experimental setup described in Ref. 39 and illustrated in Fig. 1.

The plasma source is a nanosecond-pulsed, pin-to-pin discharge housed in a 67 mm cubic vessel. The two pin-type electrodes are made of stainless steel. They are conical in shape with a parabolic tip, with an approximate radius of curvature of 500 μm.[40] They are fixed at 3 mm separation. The plasma produced between them has a radius of roughly 1 mm. Assuming the discharge to be approximately cylindrical, the initial plasma volume is 9.42×10^{-3} cm^3. The volume of the vessel is 300 cm^3 and the plasma is generated at its center, meaning that interactions with the plasma and vessel walls are negligible and the surface area of the vessel is ignored in the model. The surface area in contact with the plasma is instead set to 0.0524 cm^2, the approximate area of the parabolic electrode tips that bulk plasma emission extends across. A helium feed gas with a 0.25% water vapor admixture, equivalent to 2500 parts-per-million by volume, is supplied to the vessel.

The width and amplitude of the power profile are based on current and voltage measurements of the physical setup, with a typical pulse shown in Fig. 2. The scheme utilizes a negative voltage pulse with an amplitude of 2.5 kV, a rise time of 3 ns, and a duration of roughly 80 ns. Plasmas generated in this manner have been observed to be reasonably homogeneous along the discharge channel.[39] It is, therefore, expected that the 0D model described above will provide a good approximation of the plasma chemistry. The current and voltage signals are multiplied together to find the power supplied to the plasma over time, before being simplified slightly to streamline the model input. The experimentally measured pulse and its approximation are also shown in Fig. 2. The power deposition used in the model is 0 outside the width of the simplified profile. The duration of power deposition is 89 ns per cycle, with a rise time to peak of 67 ns. The pulse amplitude and

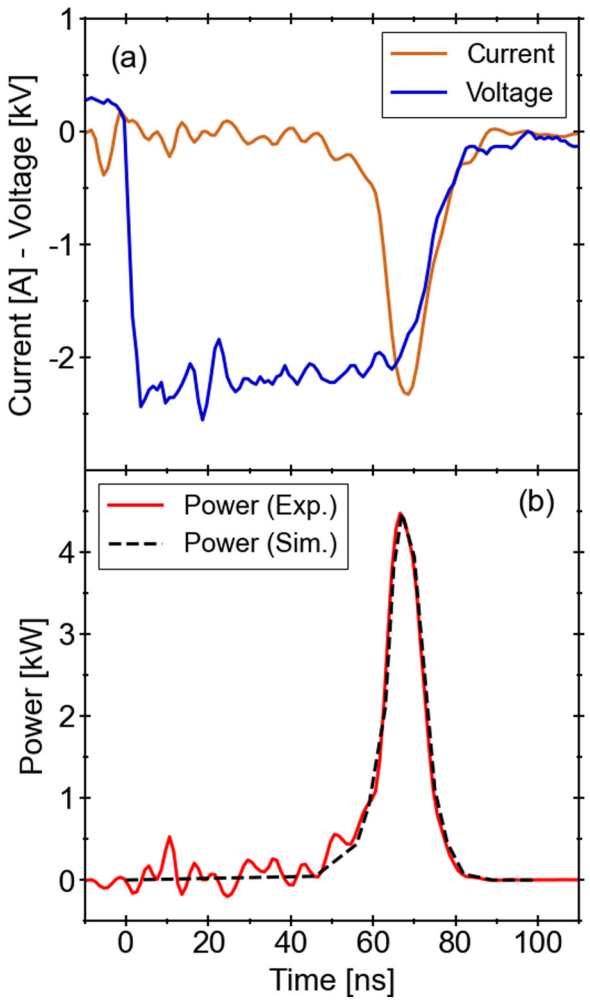

FIG. 2. (a) Characteristic current and voltage signals supplied by a ns-pulsed negative voltage generator, and (b) an experimental power profile overlaid with a simplified version used in the model.

duration are kept constant for all repetition frequencies. As such, by altering the pulse repetition frequency, the afterglow is the phase of the cycle that is modified. The use of this pulse scheme produces model electron densities comparable to the experimentally measured ones presented in Ref. 39.

The pulse repetition frequency is varied in the range of 1–100 kHz. Across this frequency range, the pulse width is significantly shorter than the overall cycle time. In addition to this, the plasma chemistry during and shortly after the pulse is driven by electron interactions occurring on very short timescales, whereas the late stage of the cycle is dominated by heavy particle interactions on comparatively longer timescales. Consequently, the time steps used in the model must allow the plasma chemistry in the pulse to be captured in high resolution, while using longer time steps in the afterglow phase to relax computational demand and

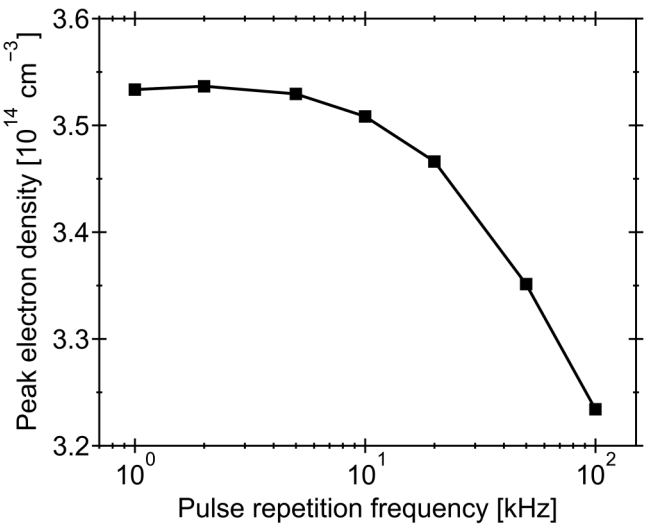

FIG. 3. Average peak electron density per cycle as a function of pulse repetition frequency.

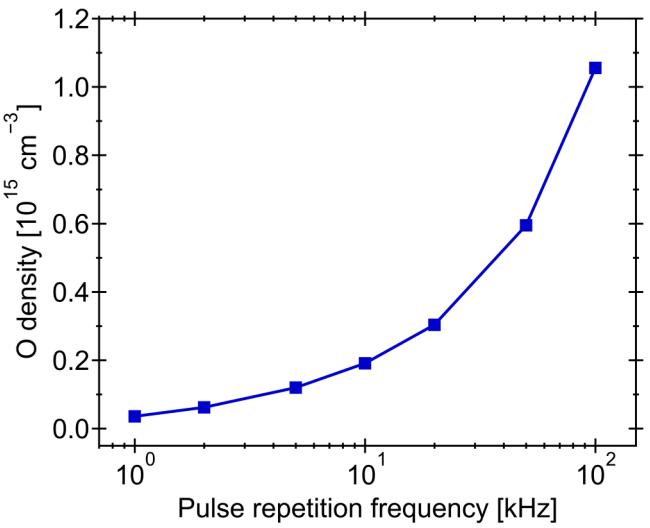

FIG. 5. Average atomic oxygen density in equilibrium as a function of pulse repetition frequency.

produce a more efficient output. This is achieved by setting each subsequent time step to increase by a constant factor determined by the given repetition frequency. The time step then resets with the following cycle.

Simulations are run until the plasma reaches an equilibrium, with the time-averaged density of a species found by taking the mean of its density across ten cycles in equilibrium. This allows a good degree of confidence in the results. For the same reason, the average peak electron density per cycle is taken as the mean of the peak electron density across ten cycles. Time-resolved measurements are taken across one cycle in equilibrium. Analysis of time-resolved parameters is achieved by normalizing the time in the cycle to the total duration of a cycle at the given repetition frequency, with $t = 0$ being the moment of maximum power deposition. Data on reaction pathways in the plasma are extracted and streamlined to find dominant reaction rates using the software package PumpKin.[41]

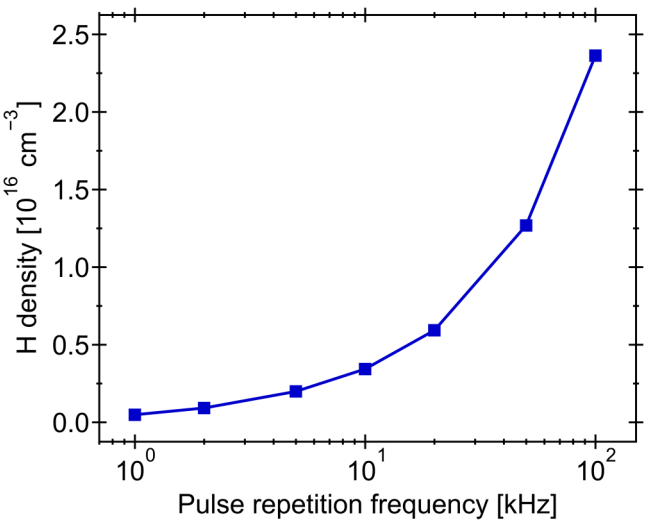

FIG. 4. Average atomic hydrogen density in equilibrium as a function of pulse repetition frequency.

III. RESULTS AND DISCUSSION

A. Electrons

The effect of pulse repetition frequency on the average peak electron density when the plasma is in equilibrium is shown in Fig. 3. The peak electron density is only weakly affected by pulse repetition frequency, changing by 9% between the maximum and minimum values recorded. This is unsurprising, as most of the electrons created by the pulse recombine on timescales significantly shorter than the cycle time.

A very small increase in the peak electron density is observed from 1 to 2 kHz. This can likely be attributed to the memory effect,[42] with its dependence on repetition frequency identified in previous studies.[24,25] Here, increasing the repetition frequency reduces the duration of the afterglow such that larger electron population remains by the end of the cycle. The presence of residual electrons at the start of the next pulse shortens the breakdown phase of the plasma and increases the peak electron density. In this case, the memory effect is near-negligible due to the rapid recombination of the electrons at all repetitions frequencies investigated. At higher frequencies, the memory effect is offset by an expansion of the plasma that arises as a result of an increased gas temperature, increasing the overall

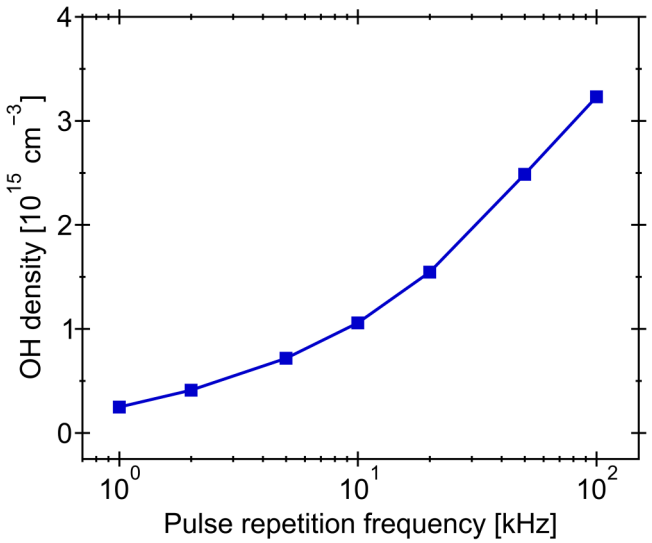

FIG. 6. Average hydroxyl density in equilibrium as a function of pulse repetition frequency.

volume occupied by the electrons and, therefore, reducing the electron density. The data presented here are in good agreement with previous experimental measurements of the pin-to-pin discharge setup modeled in this study.[39] For the same gas composition, nanosecond pulsing at a repetition frequency of 5 kHz yielded a similar electron decay curve with time. The peak spatially averaged electron density measured in those conditions was around 2.5×10^{14} cm^{-3}, which is close to 3.5×10^{14} cm^{-3} found in the present study.

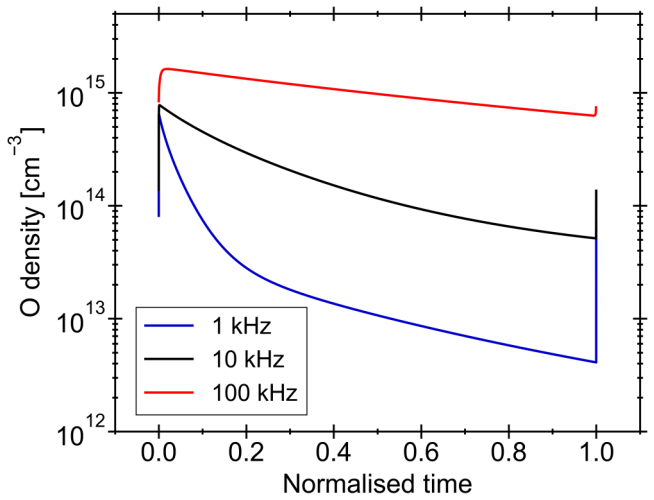

FIG. 8. Density of atomic oxygen over one cycle as a function of normalized time for different pulse repetition frequencies.

B. Radicals

Figures 4–6 show the change in time-averaged H, O, and OH densities, respectively, with pulse repetition frequency. H and O exhibit similar density trends, undergoing a minimal change at low repetition frequencies and a more substantial increase in the high frequency range. Meanwhile, OH increases more steadily with repetition frequency.

In spite of the 100-fold increase in power supplied per unit time as the pulse repetition frequency is increased from 1 to 100 kHz, the density of these radicals only increases by factors of

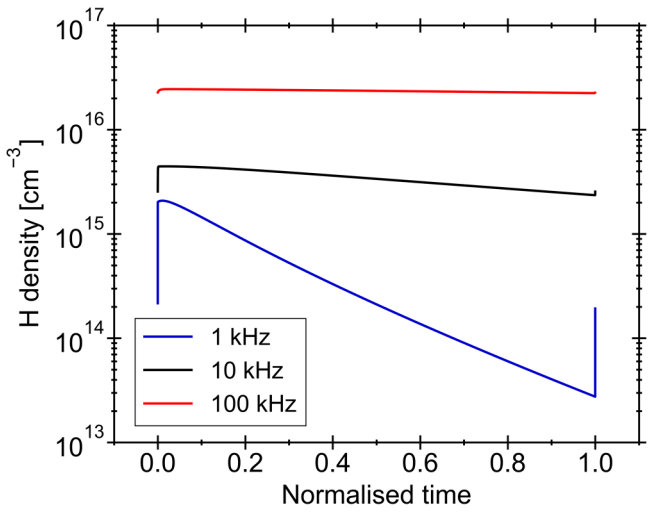

FIG. 7. Density of atomic hydrogen over one cycle as a function of normalized time for different pulse repetition frequencies.

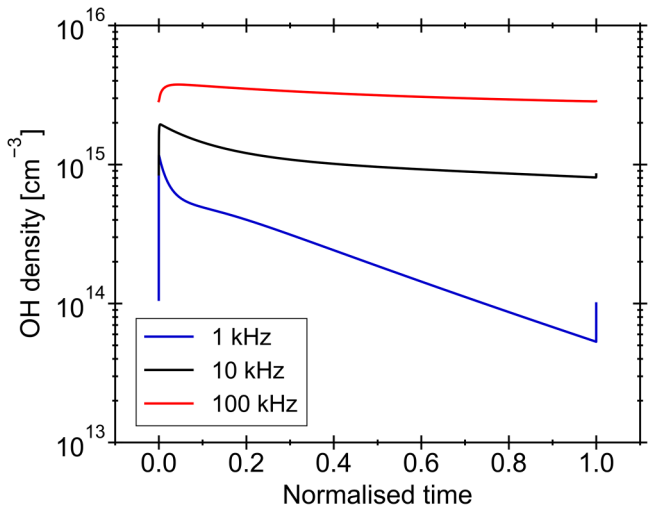

FIG. 9. Density of hydroxyl over one cycle as a function of normalized time for different pulse repetition frequencies.

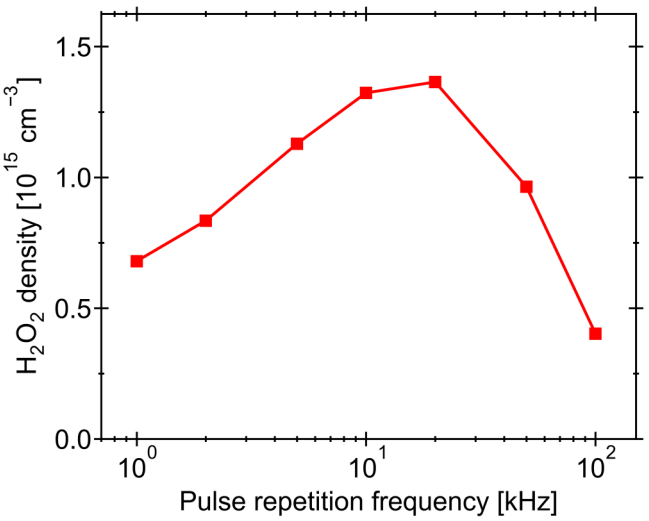

FIG. 10. Average hydrogen peroxide density in equilibrium as a function of pulse repetition frequency.

13–50. However, this is still a stark increase when compared to the electron density, especially as these species are predominantly formed through electron impact processes. To investigate this further, the densities of these radicals are plotted as a function of relative time within a cycle in Figs. 7–9. Density maxima occur shortly after the pulse for the radicals due to the associated peak in the electron density. The density of all three radicals drops substantially over the course of the afterglow at low pulse repetition frequencies. This effect is reduced toward higher repetition frequencies, where the reduced afterglow period limits the time available for the densities to decay. Indeed, once equilibrium is reached at a repetition frequency of 100 kHz, the time-resolved density of H is nearly constant. Additionally, an increase in the background gas temperature slightly enhances the radical densities in the range of 50–100 kHz.

The H, O, and OH radicals decay significantly slower than the electrons; even at lower frequencies, the electron density decays by several orders of magnitude more than that of the radicals. This leads to the radical densities experiencing a more pronounced memory effect compared to the electrons, with the latter decaying to near background densities at low repetition frequencies. In contrast, the significant radical densities remaining at the start of the next pulse further increase their peak densities until an equilibrium is reached. Similar effects were noted in a modeling study of pulsed He+O_2 plasmas, where increasing the pulse repetition frequency was found to increase the density of the O radical and the excited states O (^{1}D) and O_2($^1\Delta_g$).[26] Likewise, an increase in the H radical density with repetition frequency is also seen in Ar+CH_4 mixtures,[30,34] and an increase in OH with repetition frequency is seen in CH_4+air and H_2+air mixtures.[36,37] As with the present work, the authors of these previous studies attribute the increased radical densities to accumulation with decreasing afterglow duration. These results indicate that the afterglow period is important for determining the final densities of H, O, and OH despite their short lifetimes.

C. H_2O_2

Figure 10 shows the relationship between the pulse repetition frequency and the average H_2O_2 density. The density of H_2O_2 initially increases with the repetition frequency, before peaking at 20 kHz and dropping sharply toward 100 kHz.

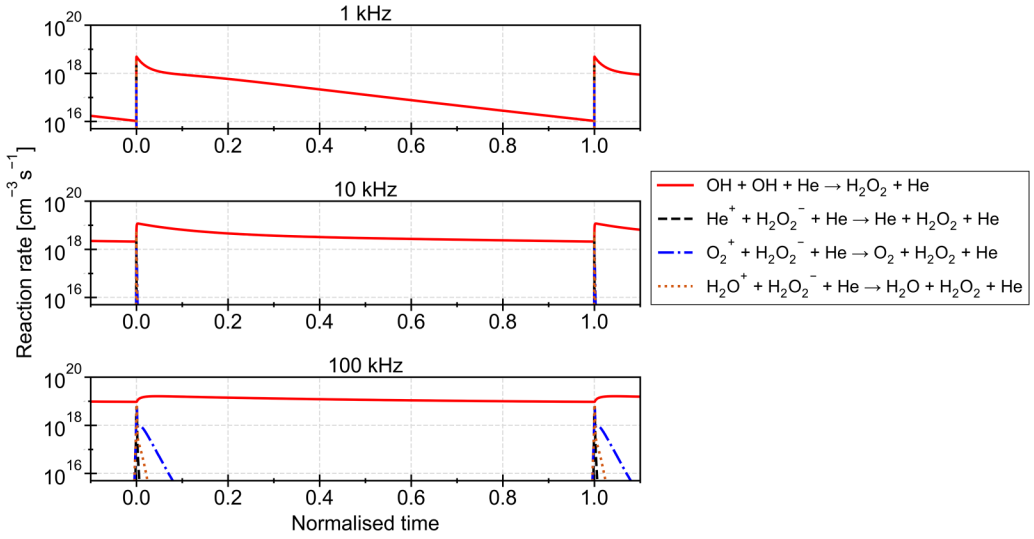

FIG. 11. Rates of dominant H_2O_2 production reactions over one cycle for 1, 10, and 100 kHz pulse repetition frequencies.

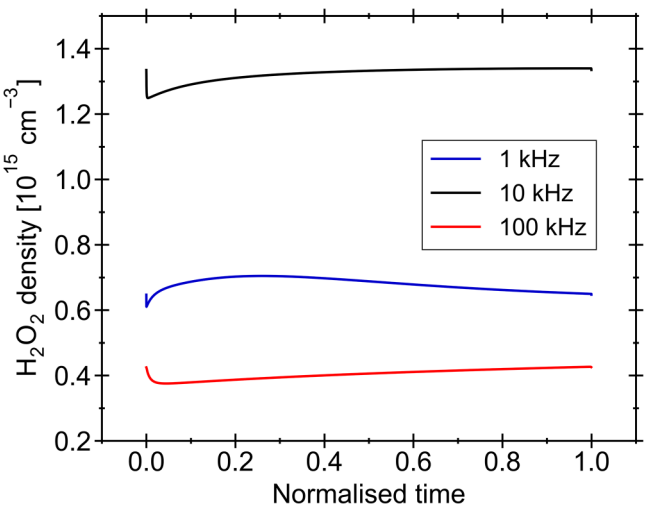

FIG. 12. Density of H_2O_2 over one cycle as a function of normalized time for different pulse repetition frequencies.

Analysis of the dominant reaction pathways is necessary to explain this trend. Figure 11 shows the change in the rate of these reactions over one cycle. For all pulse repetition frequencies modeled, H_2O_2 formation is seen to take place throughout the full cycle. This occurs predominantly through the three-body recombination of two OH radicals,

$$OH + OH + He \rightarrow H_2O_2 + He. \quad (4)$$

This reaction is generally accepted to be the main mechanism of H_2O_2 production in atmospheric pressure plasmas with water vapor admixtures.[8,43] There is also a small spike in H_2O_2-producing ion interactions close to the pulse. The peaks of these reaction rates are mostly unaffected by the pulse repetition frequency, although their duration relative to the cycle period increases as the repetition frequency is raised.

The increase in H_2O_2 density in the low repetition frequency range is likely a consequence of the steady increase in OH over the same frequency range. However, the peak and subsequent decrease in the H_2O_2 density seen at repetition frequencies above 20 kHz does not match the trend shown for OH in Fig. 6. To investigate this, Fig. 12 shows the density of H_2O_2 as a function of normalized time over one cycle in equilibrium. H_2O_2 is seen to accumulate through the early to mid afterglow at 1 kHz and throughout the full afterglow at 10 kHz and 100 kHz, primarily through OH recombination in reaction (4). Another feature of importance is the decrease in the H_2O_2 density during and shortly after the pulse.

Figure 13 shows that this is tied to a significant increase in the rates of dissociation reactions between electrons and H_2O_2 shortly after the pulse, along with an increase in the rate of H_2O_2 dissociation by the electronically excited $He(2^3S)$.[44] As the pulse repetition frequency is increased, these reactions remain at high rates for increasingly longer fractions of the cycle. Though less significant than during the pulse phase, H_2O_2 consumption is relatively consistent in the afterglow after these processes die out. The dominant contribution comes from a reaction with OH. Despite this, the consumption from OH is lower than the production from OH via reaction (4), meaning that there is still a net increase in H_2O_2 from OH. Another source of consumption is the reaction between H_2O_2 and atomic hydrogen, a process whose rate in the late afterglow increases significantly with pulse repetition frequency.

It so follows that a reduction in the afterglow period with increasing repetition frequency restricts the time available for OH to react to form H_2O_2, while also increasing the fraction of the

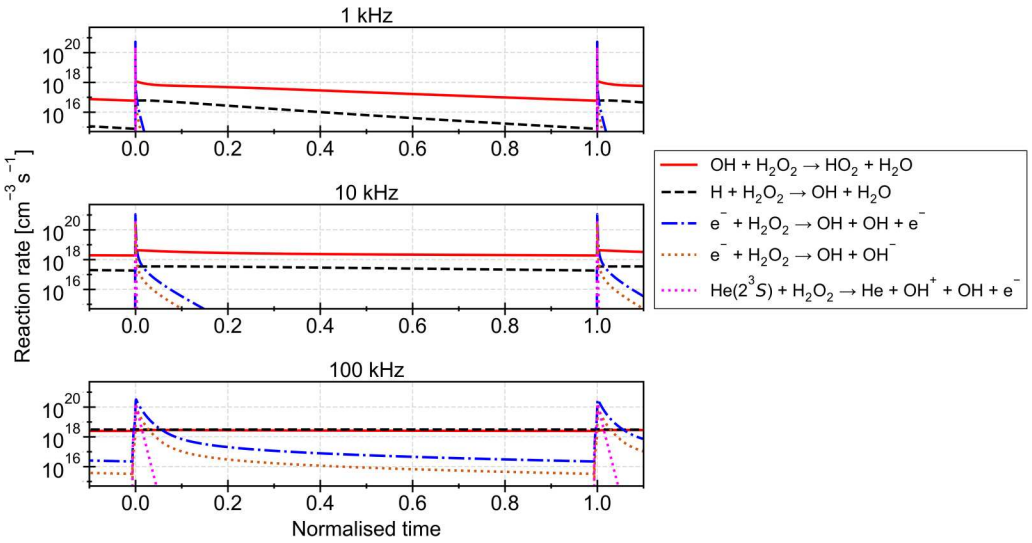

FIG. 13. Rates of dominant H_2O_2 consumption reactions over one cycle for 1, 10, and 100 kHz pulse repetition frequencies.

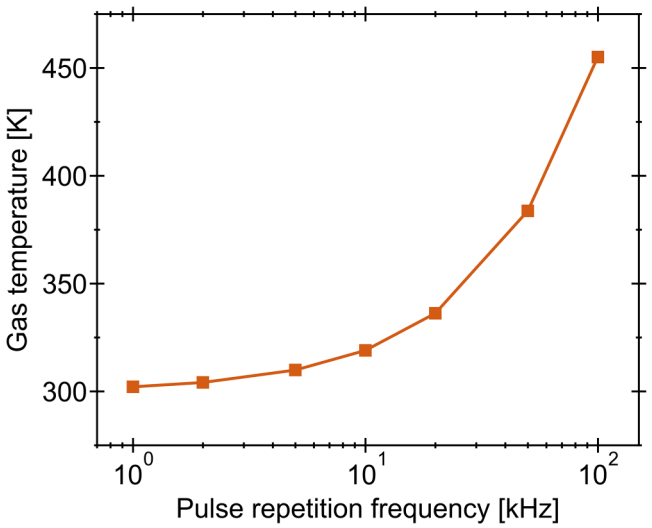

FIG. 14. Average gas temperature in equilibrium as a function of pulse repetition frequency.

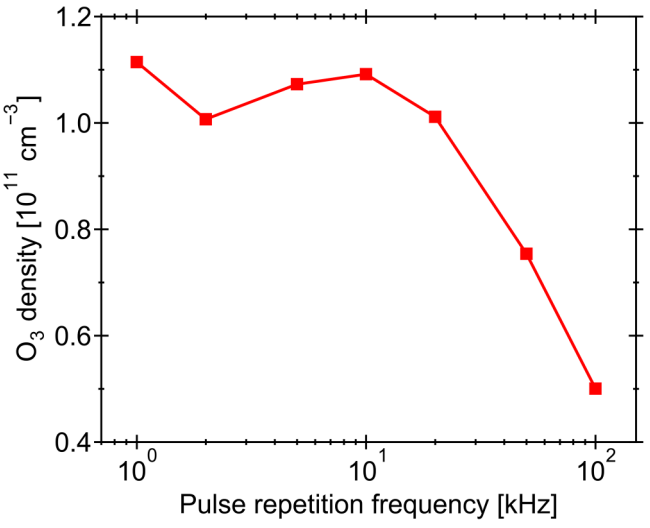

FIG. 15. Average ozone density in equilibrium as a function of pulse repetition frequency.

cycle where H_2O_2 is destroyed by electrons and metastables. This is the case despite the high OH densities seen at higher pulse repetition frequencies. It can be concluded that at the peak in H_2O_2 density at 20 kHz, the limiting factor in its production changes from OH availability at lower repetition frequencies to the afterglow duration at higher repetition frequencies. Another factor that impacts the density of H_2O_2 is the temperature of the background gas. Figure 14 shows the change in the time-averaged gas temperature with the pulse repetition frequency. It can be seen that the gas temperature increases steadily with repetition frequency, with a minimum of 300 K at 1 kHz and peaking at 455 K at 100 kHz.

H_2O_2 is known to undergo thermal decomposition at high temperatures, with this effect contributing to the drop in H_2O_2

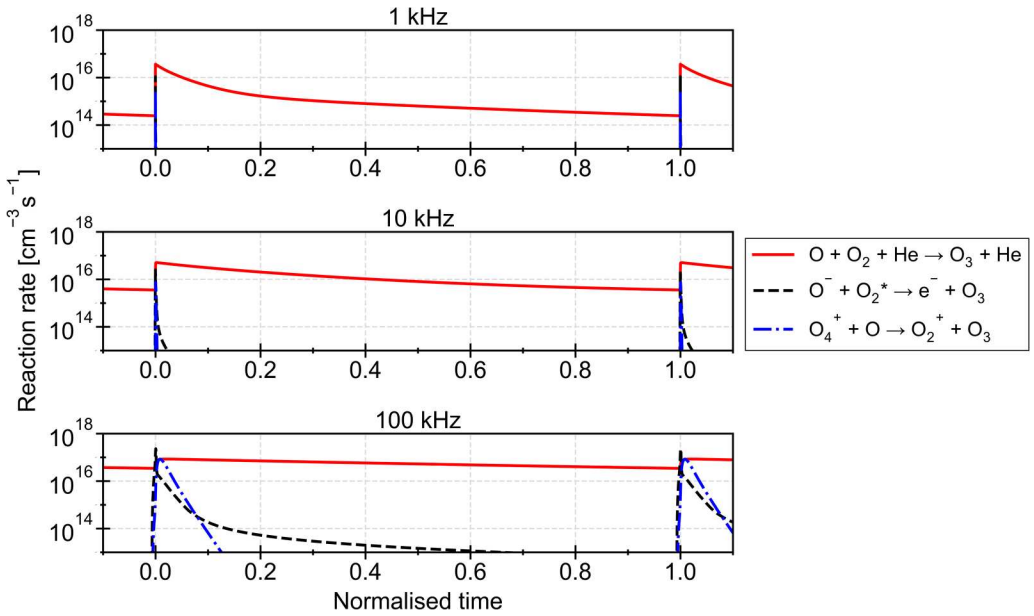

FIG. 16. Rates of dominant O_3 production reactions over one cycle for 1, 10, and 100 kHz pulse repetition frequencies.

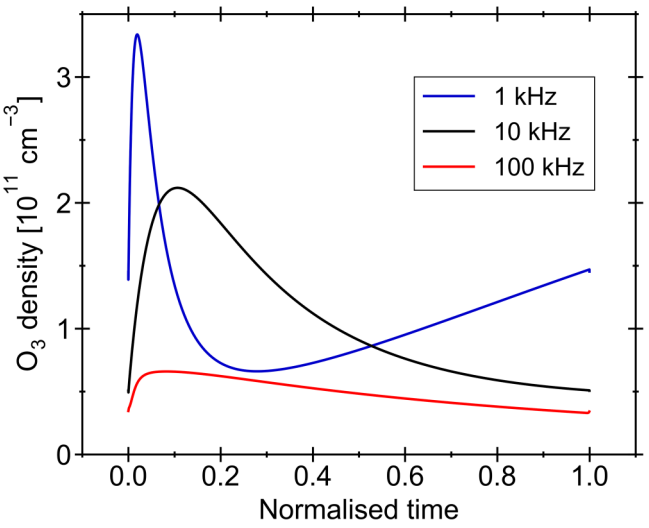

FIG. 17. Density of O_3 over one cycle as a function of normalized time for different pulse repetition frequencies.

seen above 20 kHz as the gas temperature increases appreciably in the same range.[45] Nevertheless, the influence of gas heating only exacerbates the existing trend seen for H_2O_2. Simulations with a constant gas temperature of 300 K show the same trend, albeit with the peak and drop in the H_2O_2 density shifted toward higher pulse repetition frequencies.

D. O_3

O_3 is produced in significantly lower quantities in plasmas with water vapor admixtures when compared to plasmas with admixtures of oxygen gas due to the preferential formation of hydrogen-containing species over O or O_3. Analysis of the reaction chemistry suggests that this phenomenon arises from the plasma conditions supporting hydrogen catalytic cycles, whereby hydrogen-containing radicals catalyze the decay of O and O_3 into O_2.[46,47] The densities of the radicals, namely, H, OH, and HO_2, are largely unaffected by these cycles. Figure 15 shows a complex relationship between the density of O_3 and pulse repetition frequency. The maximum O_3 density occurs at a frequency of 1 kHz, with this density dropping toward 2 kHz and rising to a second, smaller peak at 10 kHz. The O_3 density drops sharply as the repetition frequency is increased above this.

This relationship is largely influenced by the changing reaction chemistry, and therefore, the dominant mechanisms must be considered. Figure 16 shows that O_3 is predominantly formed through the three-body recombination of O and O_2 with background He,

$$O + O_2 + He \rightarrow O_3 + He. \quad (5)$$

The rate of this reaction is consistent across the full cycle at higher pulse repetition frequencies, while at low repetition frequencies, the longer afterglow duration causes the rate to drop by around two orders of magnitude by the end of the cycle as O is depleted. O_3 is also produced through ion interactions close to the pulse, with these processes increasing in rate and extending through a larger portion of the afterglow toward higher pulse repetition frequencies, although this effect becomes insignificant compared to the rising gas temperature.

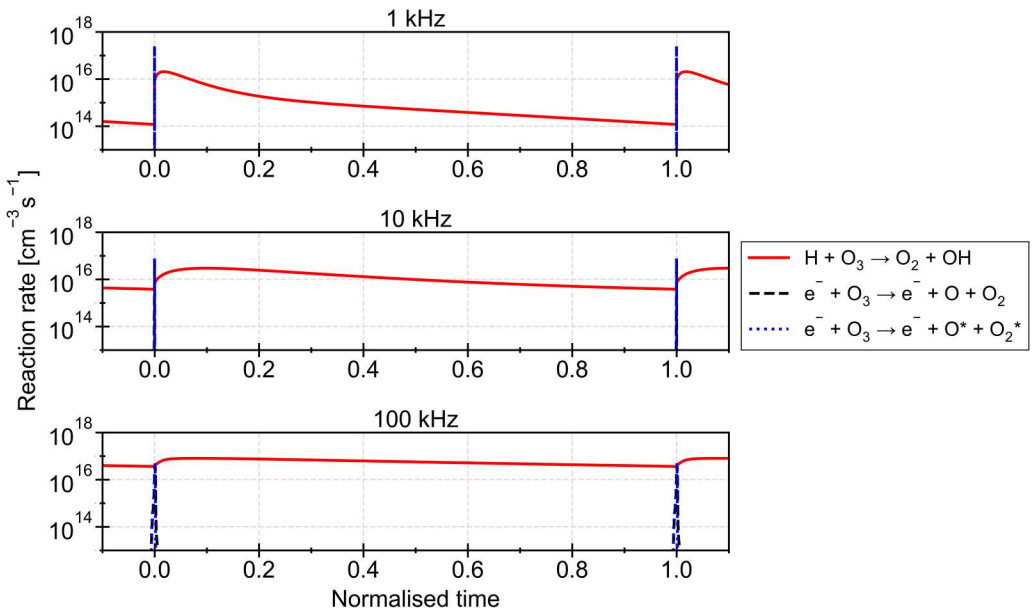

FIG. 18. Rates of dominant O_3 consumption reactions over one cycle for 1, 10, and 100 kHz pulse repetition frequencies.

Examining the change in the O_3 density over one cycle at 1, 10, and 100 kHz, given in Fig. 17, shows that the peak density of O_3 is reached shortly after the pulse. Its magnitude decreases with repetition frequency. In all cases, this peak is followed by a decline in the O_3 density. This decline persists throughout the full afterglow at 10 and 100 kHz. At 1 kHz, a minimum is reached a quarter of the way through the cycle, with the O_3 density increasing again through the remaining afterglow.

Figure 18 shows the rates of key O_3 consumption reactions during one cycle in equilibrium. The primary O_3 consumption pathway is as follows:

$$H + O_3 \rightarrow O_2 + OH. \quad (6)$$

This reaction dominates the afterglow phase because of an abundance of H atoms due largely to the electron-impact dissociation of H_2O and H_2 during the pulse. There is also a spike in electron-impact processes that destroy O_3 near the pulse. The rate of reaction (6) is dependent on afterglow duration, staying roughly constant at high repetition frequencies but dropping by two orders of magnitude in the 1 kHz case wherein the afterglow lasts for long enough for the density of H to be severely depleted. Increasing the repetition frequency also increases the overall peak rate of reaction (6). It can, therefore, be concluded that the production of O_3 seen in the afterglow at 1 kHz is due to the lack of availability of atomic hydrogen. Thus, the decrease in the average O_3 density at 2 kHz shown in Fig. 15 can be attributed to a reduction of the afterglow as compared to the 1 kHz case such that the density of H is not depleted significantly. This limits the late-afterglow buildup of O_3 at 2 kHz. The change in the O density from 1 to 2 kHz is minimal, resulting in negligible extra O_3 production from reaction (5). As the pulse repetition frequency is increased from 2 to 10 kHz, a more appreciable increase in the density of O enhances O_3 production through reaction (5), outmatching the effects of the reduced afterglow and H abundance and increasing the overall mean density. The subsequent decay seen from 10 to 100 kHz is heavily dictated by the rising gas temperature, as O_3 is highly sensitive to thermal decomposition.[48] This is corroborated by simulating the plasma with a constant background gas temperature; under these conditions, a minimum is still reached at 2 kHz and the density of O_3 rises above 10 kHz rather than decaying.

To summarize, the observed dependence of O_3 density on pulse repetition frequency results from the interplay between O and H reactant availability and afterglow duration at low frequencies, while at high frequencies, the influence of background gas heating dominates.

IV. CONCLUSION

Pulse repetition frequency shows potential as a parameter for controlling ROS production in pulsed-power He+H_2O plasmas. The changes made are electrical, thus having rapid response times and relatively convenient implementation. In this study, a pulsed-power, pin-to-pin He+H_2O plasma is modeled using GlobalKin with a PumpKin plugin. The plasma is simulated at different pulse repetition frequencies with a constant pulse shape, thus varying the duration of the afterglow phase. The plasma chemistry is subsequently analyzed with focus on biomedically relevant species and their precursors. The reduction in afterglow duration with increasing repetition frequency increases the influence of the memory effect. This results in a greater residual electron population by the end of the cycle, in turn causing a slight increase in the peak electron density at 2 kHz. However, this effect is outmatched by gas expansion in the 5–100 kHz range. The densities of short-lived species (namely H, O, and OH) decay much more slowly than the electron density, dropping by several orders of magnitude less than the electron density by the end of the cycle. This results in a more pronounced memory effect, boosting the peak radical densities until an equilibrium is reached. The density of H_2O_2 exhibits a more complex relationship with frequency as it has a comparatively longer lifetime and is mainly produced throughout the afterglow. As such, the pulse repetition frequency can be used to modulate the density of H_2O_2 provided that its relationship with this parameter is clearly understood. Finally, the density of O_3 is dependent on the afterglow duration and availability of O and H as reactants, although at high repetition frequencies, an increase in the gas temperature drives a strong O_3 decay. This work serves to highlight the importance of the pulse repetition frequency, and by extension the afterglow duration, when optimizing a pulsed plasma for biomedical applications. Though the pulse repetition frequency can indeed be used to tune the plasma composition, it is clear that the effects on the plasma chemistry are significant and a thorough understanding of the chemistry is needed to effectively utilize this parameter to optimize a plasma.

ACKNOWLEDGMENTS

The authors would like to thank Dr. Helen Davies for many productive discussions. They would also like to thank Dr. Kari Niemi and Dr. Alexandra Brisset for their help with setting up the simulations. We also acknowledge financial support from the UK EPSRC (Nos. EP/S026584/1 and EP/S025790/1) and the Norma Ann Christie Scholarship.

AUTHOR DECLARATIONS

Conflict of Interest

The authors have no conflicts to disclose.

Author Contributions

B. Harris: Conceptualization (equal); Data curation (lead); Formal analysis (lead); Investigation (lead); Methodology (equal); Validation (lead); Visualization (lead); Writing – original draft (lead); Writing – review & editing (lead). **E. Wagenaars:** Conceptualization (equal); Funding acquisition (lead); Methodology (equal); Project administration (lead); Resources (lead); Supervision (lead).

DATA AVAILABILITY

The data that support the findings of this study are openly available in the York Research Database at https://doi.org/10.15124/a16dce57-8907-457a-b2cc-5b60e7c446fc.

REFERENCES

[1]D. B. Graves, J. Phys. D: Appl. Phys. **45**, 263001 (2012).
[2]A. Brisset, A. R. Gibson, S. Schröter, K. Niemi, J.-P. Booth, T. Gans, D. O'Connell, and E. Wagenaars, J. Phys. D: Appl. Phys. **54**, 285201 (2021).
[3]S. Reuter, H. Tresp, K. Wende, M. U. Hammer, J. Winter, K. Masur, A. Schmidt-Bleker, and K.-D. Weltmann, IEEE Trans. Plasma Sci. **40**, 2986 (2012).
[4]D. Shaw, A. West, J. Bredin, and E. Wagenaars, Plasma Sources Sci. Technol. **25**, 065018 (2016).
[5]S. Klose, K. Manfred, H. Norman, G. Ritchie, and J. Van Helden, Plasma Sources Sci. Technol. **29**, 085011 (2020).
[6]S. Schröter, A. Wijaikhum, A. R. Gibson, A. West, H. L. Davies, N. Minesi, J. Dedrick, E. Wagenaars, N. De Oliveira, L. Nahon, M. J. Kushner, J.-P. Booth, K. Niemi, T. Gans, and D. O'Connell, Phys. Chem. Chem. Phys. **20**, 24263 (2018).
[7]J. Dedrick, S. Schröter, K. Niemi, A. Wijaikhum, E. Wagenaars, N. de Oliveira, L. Nahon, J.-P. Booth, D. O'Connell, and T. Gans, J. Phys. D: Appl. Phys. **50**, 455204 (2017).
[8]D.-X. Liu, P. Bruggeman, F. Iza, M.-Z. Rong, and M. G. Kong, Plasma Sources Sci. Technol. **19**, 025018 (2010).
[9]X. Zimu, L. Yan, M. Jie, S. Jie, H. Wei, H. Shuheng, Y. Chaobing, X. Wenhao, Y. Zhang, Y. Chunjun, Z. Xiao, and C. Cheng, Plasma Sci. Technol. **22**, 103001 (2020).
[10]I. Niedźwiedź, A. Waśko, J. Pawłat, and M. Polak-Berecka, Pol. J. Microbiol. **68**, 153 (2019).
[11]S. K. Dubey, S. Parab, A. Alexander, M. Agrawal, V. P. K. Achalla, U. N. Pal, M. M. Pandey, and P. Kesharwani, Process Biochem. **112**, 112 (2022).
[12]M. Schieber and N. S. Chandel, Curr. Biol. **24**, R453 (2014).
[13]C. Lennicke, J. Rahn, R. Lichtenfels, L. A. Wessjohann, and B. Seliger, Cell Commun. Signal. **13**, 39 (2015).
[14]J. Kanta, Acta Medica (Hradec Kralove) **54**, 97 (2011).
[15]B. Haertel, T. Von Woedtke, K.-D. Weltmann, and U. Lindequist, Biomol. Ther. **22**, 477 (2014).
[16]D. Ellerweg, J. Benedikt, A. von Keudell, N. Knake, and V. Schulz-von der Gathen, New J. Phys. **12**, 013021 (2010).
[17]T. Murakami, K. Niemi, T. Gans, D. O'Connell, and W. G. Graham, Plasma Sources Sci. Technol. **22**, 015003 (2012).
[18]S. Kelly and M. M. Turner, Plasma Sources Sci. Technol. **23**, 065013 (2014).
[19]A. Wijaikhum, D. Schröder, S. Schröter, A. R. Gibson, K. Niemi, J. Friderich, A. Greb, V. Schulz-von der Gathen, D. O'Connell, and T. Gans, Plasma Sources Sci. Technol. **26**, 115004 (2017).
[20]G. Willems, J. Benedikt, and A. Von Keudell, J. Phys. D: Appl. Phys. **50**, 335204 (2017).
[21]D. Liu, F. Iza, X. Wang, M. Kong, and M. Rong, Appl. Phys. Lett. **98**, 221501 (2011).
[22]K. McKay, D.-X. Liu, M.-Z. Rong, F. Iza, and M. G. Kong, J. Phys. D: Appl. Phys. **45**, 172001 (2012).
[23]S. Tao, L. Kaihua, Z. Cheng, Y. Ping, Z. Shichang, and P. Ruzheng, J. Phys. D: Appl. Phys. **41**, 215203 (2008).
[24]J. Walsh, P. Olszewski, and J. Bradley, Plasma Sources Sci. Technol. **21**, 034007 (2012).
[25]Y. Liu, H. Yan, H. Guo, Z. Fan, Y. Wang, Y. Wu, and C. Ren, Phys. Plasmas **25**, 033519 (2018).
[26]G. Pan, Z. Tan, J. Pan, X. Wang, and C. Shan, Phys. Plasmas **23**, 043508 (2016).
[27]H. K. Song, H. Lee, J.-W. Choi, and B.-K. Na, Plasma Chem. Plasma Process. **24**, 57 (2004).
[28]H. Min Joh, S. Ja Kim, T. Chung, and S. Leem, Appl. Phys. Lett. **101**, 053703 (2012).
[29]S. A. Norberg, G. M. Parsey, A. M. Lietz, E. Johnsen, and M. J. Kushner, J. Phys. D: Appl. Phys. **52**, 1 (2018).
[30]B. Huang, C. Zhang, H. Sun, D. A. Sorokin, V. F. Tarasenko, and T. Shao, Plasma Sources Sci. Technol. **31**, 025019 (2022).
[31]S. Shen, J. Yan, Y. Wang, Y. Wang, W. Ding, and G. Sun, Plasma Sources Sci. Technol. **31**, 105003 (2022).
[32]S. Adams, J. Miles, T. Ombrello, R. Brayfield, and J. Lefkowitz, J. Phys. D: Appl. Phys. **52**, 355203 (2019).
[33]Y. Li, H. Li, Z. Liu, Y. Fu, H. Luo, X. Zou, and X. Wang, Phys. Plasmas **28**, 073510 (2021).
[34]B. Huang, C. Zhang, C. Zhang, and T. Shao, J. Phys. D: Appl. Phys. **56**, 095201 (2023).
[35]B.-D. Huang, K. Takashima, X.-M. Zhu, and Y.-K. Pu, J. Phys. D: Appl. Phys. **47**, 422003 (2014).
[36]X. Mao, H. Zhong, Z. Wang, T. Ombrello, and Y. Ju, Proc. Combust. Inst. **39**, 5457 (2023).
[37]J. K. Lefkowitz, S. D. Hammack, C. D. Carter, and T. M. Ombrello, Proc. Combust. Inst. **38**, 6671 (2021).
[38]A. M. Lietz and M. J. Kushner, J. Phys. D: Appl. Phys. **49**, 425204 (2016).
[39]A. Brisset, B. Harris, A. Dickenson, K. Niemi, J. Walsh, and E. Wagenaars, Plasma Sources Sci. Technol. **31**, 045008 (2022).
[40]A. Brisset, M. Bieniek, L. Invernizzi, M. Hasan, J. Walsh, K. Niemi, and E. Wagenaars, Plasma Sources Sci. Technol. **32**, 065004 (2023).
[41]A. H. Markosyan, A. Luque, F. J. Gordillo-Vázquez, and U. Ebert, Comput. Phys. Commun. **185**, 2697 (2014).
[42]J. Jiang and P. J. Bruggeman, Plasma Sources Sci. Technol. **30**, 105007 (2021).
[43]B. R. Locke and K.-Y. Shih, Plasma Sources Sci. Technol. **20**, 034006 (2011).
[44]G. Nayak, N. Sadeghi, and P. J. Bruggeman, Plasma Sources Sci. Technol. **28**, 125006 (2019).
[45]P. Pędziwiatr, F. Mikołajczyk, D. Zawadzki, K. Mikołajczyk, and A. Bedka, Acta Innov. **26**, 45 (2018).
[46]D. Lary, J. Geophys. Res.: Atmos. **102**, 21515, https://doi.org/10.1029/97JD00912s (1997).
[47]I. Larin, Izv. Atmos. Ocean. Phys. **58**, 150 (2022).
[48]S. W. Benson and A. E. Axworthy, Jr., J. Chem. Phys. **26**, 1718 (1957).